

Tris-*o*-phenylenedioxytriposphazene (TPP) Inclusion Compounds Containing a Dipolar Molecular Rotor

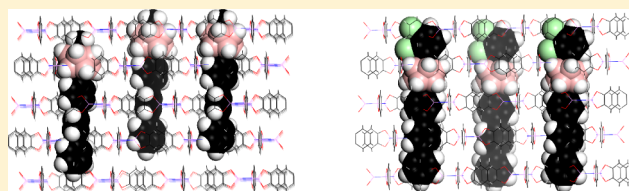
Lukáš Kobr,[†] Ke Zhao,[‡] Yongqiang Shen,[‡] Richard K. Shoemaker,[†] Charles T. Rogers,[‡] and Josef Michl^{*,†,§}

[†]Department of Chemistry and Biochemistry and [‡]Department of Physics, University of Colorado, Boulder, CO 80309, United States

[§]Institute of Organic Chemistry and Biochemistry, Academy of Sciences of the Czech Republic, 16610 Prague 6, Czech Republic

S Supporting Information

ABSTRACT: A rod-shaped molecular rotor consisting of a *p*-terphenyl shaft attached to *p*-carborane whose antipodal position carries a dipolar 2,3-dichlorophenyl rotator forms an inclusion compound with hexagonal tris-*o*-phenylenedioxytriposphazene (TPP). Results of solid-state NMR spectroscopy, X-ray powder diffraction, dielectric loss spectroscopy, and density functional theory calculations lead us to propose that the whole molecule inserts into the TPP channels, with the rotor located in the outermost surface layer. Although the placement and alignment of the dipoles at the surface appear favorable, the sample does not exhibit collective behavior even at 7 K, presumably due to the relatively large barrier to rotation (~8.6 kcal/mol). In incompletely annealed samples of the inclusion compound, some of the rotators protrude outside the surface and have a rotational barrier of ~3.4 kcal/mol. In the inclusion compound of an analog in which the rotator is replaced with a methyl group, some of the methyl substituents are located inside the surface layer of TPP and others protrude above it.



INTRODUCTION

Artificial molecular rotors^{1–7} have received considerable attention. Collections of dipolar rotors have been examined in three-dimensional (3D) crystals^{8–10} and on two-dimensional (2D) surfaces as individual rotors^{11–14} or as random assemblies^{15–18} but not in regular 2D arrays, which are of particular interest to us. Such arrays should be capable of exhibiting collective behavior, and ferroelectricity¹⁹ would be particularly desirable. A ferroelectric ground state requires a suitable regular array of rotors with low barrier to rotation (low Debye temperature) and strong ferroelectric inter-rotor interaction (high Curie temperature).

One possible approach to regular arrays of molecular rotors is based on the separation of the design of the rotor molecules themselves (high dipole, low rotational barrier) from the design of the lattice that defines their locations (small lattice constant, triangular array). This has led us to examine surface inclusion compounds of tris-*o*-phenylenedioxytriposphazene (TPP).^{20–22} The hexagonal phase of this layered material²³ (Figure 1) tends to form platelets whose large faces are parallel to the ~0.5 nm thick layers and perpendicular to a set of roughly hexagonal channels that run through the crystal. The channels have a triangular cross-section within each layer, with the triangles rotated by 60° between neighboring layers. They are arranged in a triangular pattern, about 1.1 nm apart. Their internal diameter is ~0.5 nm, and they can easily accommodate alkane chains or polyphenylenes.

The molecular rotors that are to be inserted into the channels consist of a shaft with affinity for channel interior, a stopper that is meant to be too large to fit inside the channel,

and an axle that carries a dipolar rotator and is supposed to orient itself normal to the surface on its outside. Presently, we work with the nonpolar rotor **1** and polar rotor **2** (Scheme 1), where the shaft is *p*-terphenyl, the stopper is *p*-carborane, and the rotator is either the nonpolar methyl (**1**) or the dipolar 2,3-dichlorophenyl (**2**; the dipole moment of *o*-dichlorobenzene is 2.51 D²⁴).

TPP offers many advantages, in particular a small interchannel distance, but also has two disadvantages: (i) in addition to existing in the desirable hexagonal form, it is capable of existing in a nearly equally stable monoclinic form that has no channels, accepts no guest molecules, and whose formation needs to be carefully avoided and (ii) being a molecular rather than a covalent crystal, the hexagonal form has the ability to adjust the size of its channels to accommodate even guest molecules that are larger than the empty channels, complicating the choice of the stopper part of the molecular rotor.

The principal tool that we use to characterize the rotation of dipolar rotors is dielectric spectroscopy, the measurement of capacitor dielectric loss peaks as a function of temperature. These loss peaks show dispersion with measurement frequency, indicative of a situation where the dipole moments move in a potential with activation barriers. For temperatures sufficiently high, thermal motion over the barriers allows the dipole moment to align itself with applied electric field essentially instantaneously and these dipoles then do not contribute to the

Received: September 11, 2013

Revised: December 1, 2013

Published: January 24, 2014



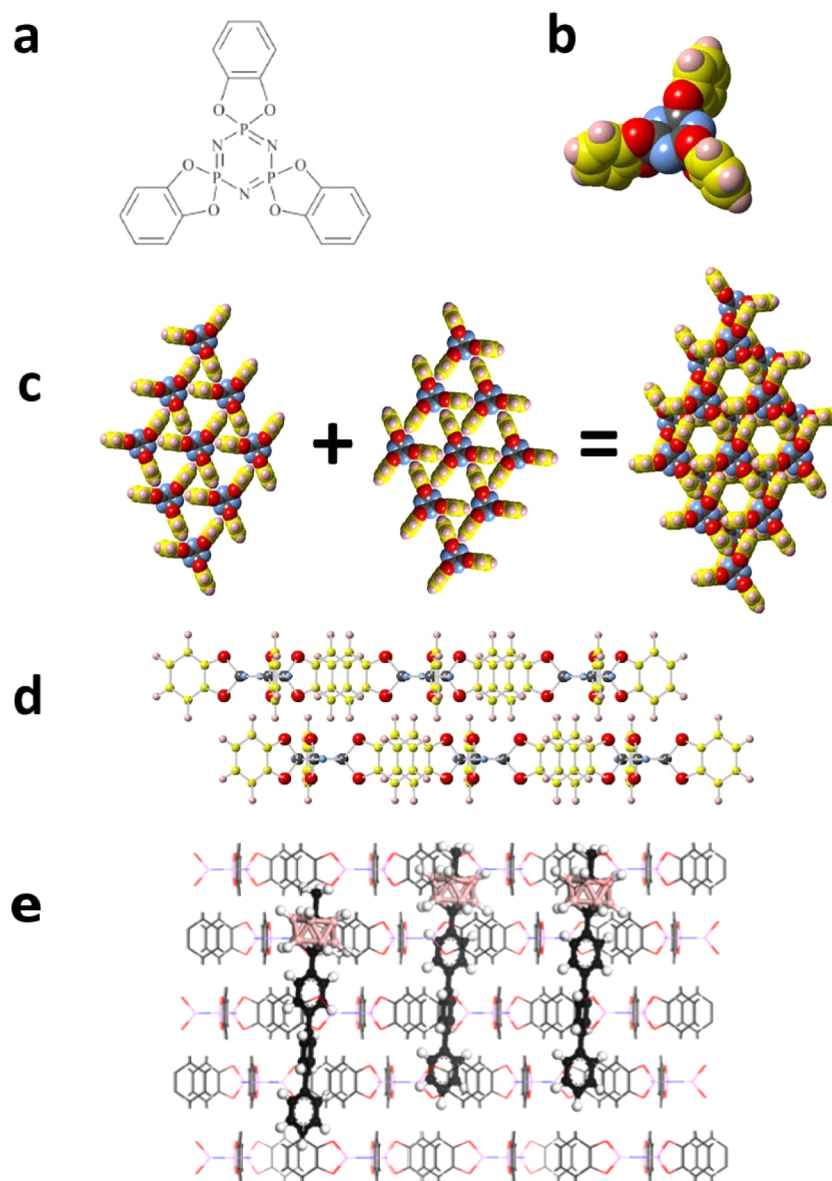


Figure 1. Crystal structure of hexagonal TPP. (a) Chemical structure and (b) space-filling model of a TPP molecule; two successive layers of a crystal viewed from the (c) top and (d) side; two anticipated modes of (e) rotor insertion.

dielectric loss. For low enough temperatures, the dipoles are frozen into wells and cannot contribute to the dielectric loss either. At intermediate temperatures, where the measurement frequency is equal to the typical thermally activated rate, dipole motion phase lags behind the applied field and leads to energy dissipation. For a simple thermal activation model of dielectric loss in a system with a density n of dipole moments of magnitude p in a double well with a barrier height E_B and an asymmetry s , the loss tangent is expected to be given by^{25–27}

$$\tan \delta = (4p_0^2 n / 9\epsilon_0 k_B T) \cosh^{-2}(s/2k_B T) [\omega\tau / (1 + \omega^2\tau^2)]$$

In this expression, k_B is the Boltzmann constant and τ is the inverse of the attempt frequency,

$$\tau = \tau_0 \exp(E_B/k_B T)$$

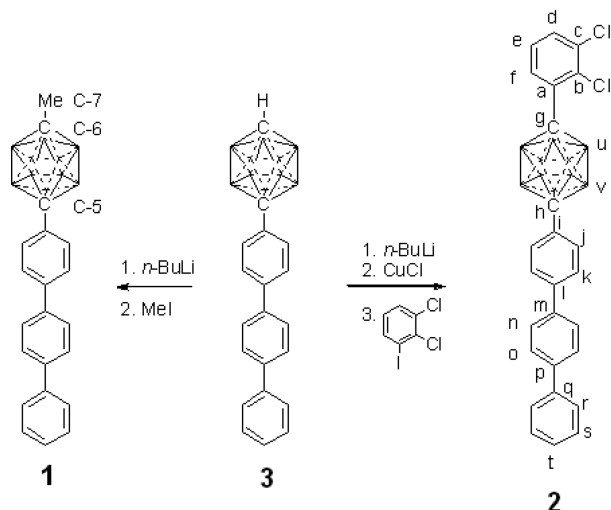
These equations predict a peak in dielectric losses whenever the choice of measurement frequency ω and temperature T is such that $\omega\tau = 1$. Thus, a plot of the inverse of observed temperature where losses peak versus the logarithm of the

measurement frequency allows us to extract estimates of average rotational barrier height E_a and prefactor τ_0 . Detailed fitting of the peak shape versus temperature and frequency allows us to extract the barrier asymmetry s and to estimate the distribution of activation energies.

RESULTS

Synthesis. 1-Methyl-12-(4-terphenyl)-*p*-carborane (**1**) was prepared in 79% yield by deprotonation and methylation of the known²² 1-(4-terphenyl)-*p*-carborane (**3**). Deprotonation of **3** followed by transmetalation with cuprous chloride and Ullmann coupling with 1,2-dichloro-3-iodobenzene afforded 1-(2,3-dichlorophenyl)-12-(4-terphenyl)-*p*-carborane **2** in 96% yield. The preparation of **2-d**₁₃ proceeded similarly starting from 4-iodo-*p*-terphenyl-*d*₁₃ (**4**), which was obtained by iodination of *p*-terphenyl-*d*₁₄.

Inclusion Compounds. A mixture of the molecular rotor and empty hexagonal TPP-*d*₁₂²⁸ was subjected to alternating ball milling and annealing to 70–75 °C, yielding the desired

Scheme 1. Synthesis of **1** and **2**

inclusion compounds, which we label with symbols such as 15%**1**@TPP-*d*₁₂ (a 15% molar mixture of **1** in fully deuteriated TPP). The inclusion compound het-15%**2**@TPP-*d*₁₂ was prepared by ball milling empty hexagonal TPP-*d*₁₂ and **2** (17:3 molar ratio) without subsequent annealing.

Differential Scanning Calorimetry (DSC). The DSC traces of **1** and 15%**1**@TPP-*d*₁₂ are shown in Figure S1 of the Supporting Information. Neat **1** (Figure S1a of the Supporting Information) shows a single endotherm at 262 °C, whereas 15%**1**@TPP-*d*₁₂ shows two endotherms at 233 and 275 °C and a sharp exotherm at 235 °C (Figure S1b of the Supporting Information). The DSC trace of hexagonal TPP-*d*₁₂ (Figure S2a of the Supporting Information) closely resembles the reported²⁹ DSC curve of hexagonal TPP and consists of a broad exotherm centered around 148 °C (first order transition of hexagonal to monoclinic TPP) and endotherms at 222 °C (first order transition of monoclinic to hexagonal TPP) and 252 °C (melting). The neat rotor **2** (Figure S2b of the Supporting Information) shows a single endotherm at 234 °C, and 15%**2**@TPP-*d*₁₂ (Figure S2c of the Supporting Information) shows a broad exotherm around 200 °C and an endotherm at 286 °C. Other than a small endotherm associated with melting TPP-*d*₁₂, the endotherms in the DSC traces of the inclusion compounds are due to their melting. The trace of 15%**2**@TPP-*d*₁₂ also shows a very small endotherm at 236 °C that is associated with the first order transition of monoclinic TPP-*d*₁₂ into its hexagonal form.

X-ray Powder Diffraction. Figure 2 shows X-ray powder diffraction patterns taken with Cu K α 1 radiation for 15%**1**@TPP-*d*₁₂ and 15%**2**@TPP-*d*₁₂. The data sets are fitted to a hexagonal model that includes a scattering background from the capillary sample holder and line width broadening due to the finite powder particle size. Both sets are consistent with an overall hexagonal structure. Mixtures containing less than the 15% molar concentration of the guest generally display powder patterns that show a complicated superposition of expanded hexagonal, empty hexagonal, and monoclinic structure of TPP.

The 15%**1**@TPP-*d*₁₂ fitting results indicate an in-plane lattice parameter of 1.2094 ± 0.0004 nm and a bilayer spacing of 1.0045 ± 0.0004 nm. The former is expanded by over 4%, and the latter is slightly contracted compared to empty TPP.²⁸ The particle size extracted from the observed X-ray peak widths is 22.5 ± 0.5 nm. The het-15%**2**@TPP-*d*₁₂ fitting results show a

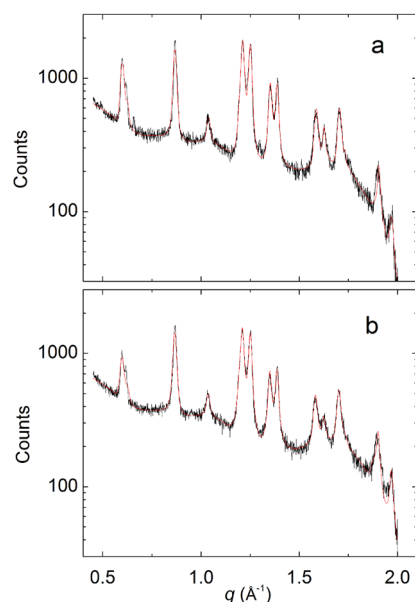


Figure 2. X-ray powder diffraction patterns (X-ray counts vs magnitude of the scatter wave vector q , black) and fitting to a hexagonal structure (red) for (a) 15%**1**@TPP-*d*₁₂ and (b) 15%**2**@TPP-*d*₁₂.

nearly identical expanded hexagonal structure with an in-plane lattice parameter of 1.2122 ± 0.0004 nm, bilayer spacing of 1.0044 ± 0.0004 nm, and particle size of 20 ± 0.3 nm (for a homogeneous 10%**2**@TPP-*d*₁₂ sample, which contained a significant amount of monoclinic TPP, the in-plane lattice parameter in the hexagonal phase was 1.2169 ± 0.0004 nm).

Solid-State NMR (ssNMR). The ³¹P cross-polarization magic angle spinning (CP MAS) ssNMR spectra (**1**: Figure S3a of the Supporting Information, **2**: Figure S3c of the Supporting Information) and the ³¹P single-pulse excitation magic angle spinning (SPE MAS) ssNMR spectra (**1**: Figure S3b of the Supporting Information, **2**: Figure S3d of the Supporting Information) of 15%**1**@TPP-*d*₁₂ and 15%**2**@TPP-*d*₁₂ all contain a single resonance at 34.0 ppm. This is compatible with the pure hexagonal structure found by XRD as monoclinic TPP exhibits three distinct resonances in its ³¹P ssNMR spectrum at 32.0, 35.1, and 38.3 ppm.³⁰

The solid-state ¹³C CP MAS NMR of neat **1** (5 ms contact time, Figure 3a) shows five resolved quaternary aromatic carbon peaks between 133 and 140 ppm, unresolved protonated aromatic carbon signals between 123 and 130 ppm, a peak for each carborane carbon (76.2 and 79.5 ppm), and a peak of the methyl carbon (26.4 ppm). The solution ¹³C NMR spectrum of **1** in CDCl₃ (Figure 3b) shows all the signals resolved. The CP MAS ssNMR spectrum of 15%**1**@TPP-*d*₁₂ obtained with 5 ms contact time, dipolar dephasing (DPD), and total sideband suppression (TOSS) (Figure 3c) greatly attenuates protonated carbons, making quaternary carbon signals stand out, while the ¹³C CP MAS ssNMR spectrum of 15%**1**@TPP-*d*₁₂ obtained with a 5 ms contact time (Figure 3d) shows both protonated and quaternary carbons.

The five quaternary aromatic carbons in **1** give rise to three peaks in the ¹³C CP MAS ssNMR spectra of 15%**1**@TPP-*d*₁₂ (C-1, C-2, and C-3, Figure 3, panels c and d). The carborane carbons give rise to two peaks (C-5 and C-6) in all spectra. All the aromatic and carborane signals in the ¹³C ssNMR spectra of 15%**1**@TPP-*d*₁₂ show a strong upfield shift of about 1.0 to 1.9

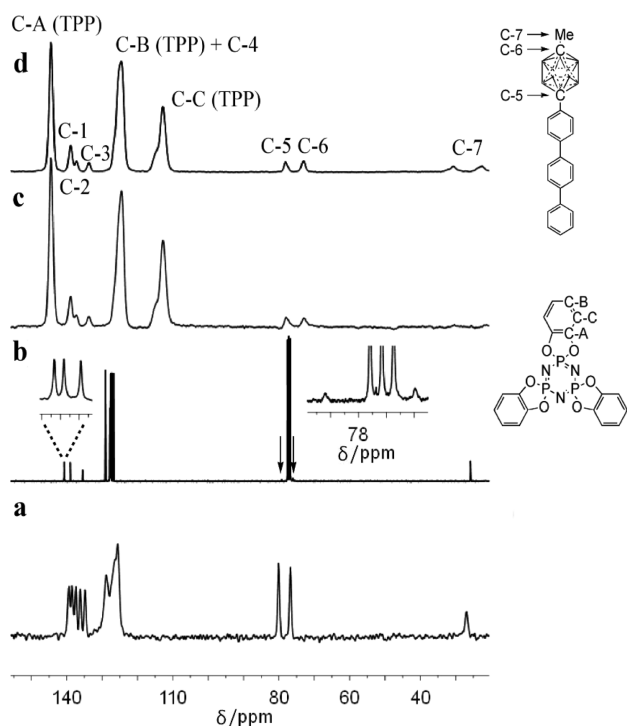


Figure 3. NMR spectra of **1**: (a) ^{13}C CP MAS, neat solid; (b) ^{13}C NMR in CDCl_3 solution; (c) ^{13}C CP MAS solid $15\%\mathbf{1}@TPP-d_{12}$ with DPD and TOSS; and (d) ^{13}C CP MAS solid $15\%\mathbf{1}@TPP-d_{12}$.

ppm relative to the solution spectrum (Table 1). The protonated aromatic carbons of $15\%\mathbf{1}@TPP-d_{12}$ also exhibit a strong upfield shift, and they overlap with the carbon C–B of $TPP-d_{12}$. The methyl signal in the spectrum of $15\%\mathbf{1}@TPP-d_{12}$ exhibits two separate broad peaks. One of them is shifted upfield by 3.2 ppm and the other one downfield by 4.8 ppm with respect to the solution spectrum of **1**.

The NMR signals in **2** were assigned using $^1\text{H} - ^{13}\text{C}$ gCOSY (Figure S4 of the Supporting Information, top), $^1\text{H} - ^{13}\text{C}$ gHSQC (Figure S4 of the Supporting Information, bottom), ^1H NMR, boron-decoupled $^1\text{H} - ^{13}\text{C}$ gHMBC NMR ($J = 8$ Hz; Figure S5a of the Supporting Information, $J = 18$ Hz; Figure S5, panels b and c, of the Supporting Information), ^{13}C NMR, and DEPT-135.

The ^{13}C NMR CP MAS ssNMR spectrum of neat **2** (Figure 4a) was recorded using a 5 ms contact time, and it shows a series of broad largely overlapping peaks in the aromatic region, and a distinct peak for each *p*-carborane carbon at 82.7 and 87.5 ppm. The solution ^{13}C NMR spectrum of **2** (Figure 4b) shows all the peaks resolved and the *p*-terphenyl resonances have nearly the same chemical shifts as in the solution ^{13}C NMR spectrum of **1**.

In addition to the three intense aromatic singlet resonances associated with hexagonal $TPP-d_{12}$, the ^{13}C CP MAS ssNMR spectrum of $15\%\mathbf{2}@TPP-d_{12}$ (Figure 4c) displays a series of aromatic resonances associated with the *p*-terphenyl unit and identical to those in the ^{13}C spectrum of $15\%\mathbf{1}@TPP-d_{12}$. The

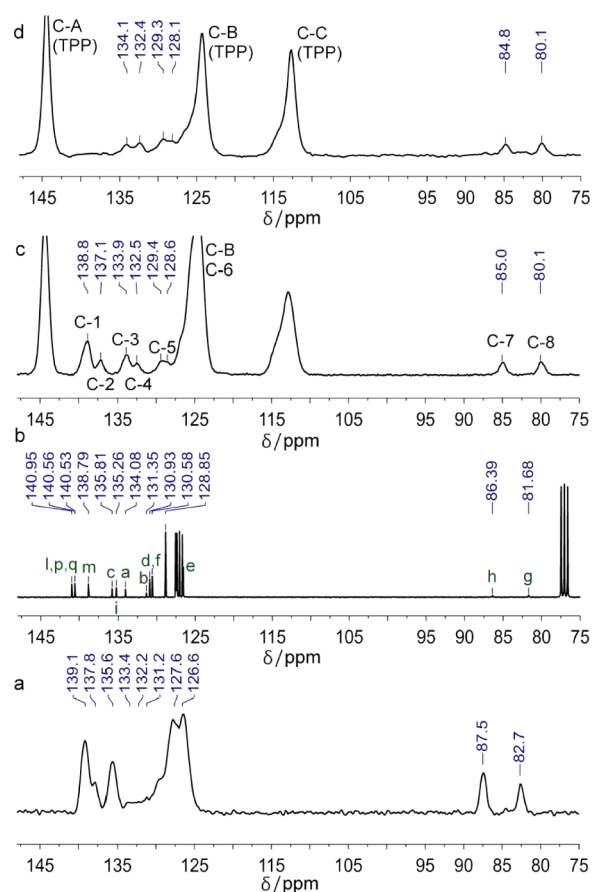


Figure 4. NMR spectra of **2**: (a) ^{13}C CP MAS neat solid, (b) ^{13}C in CDCl_3 solution, (c) ^{13}C CP MAS solid $15\%\mathbf{2}@TPP-d_{12}$, and (d) ^{13}C CP MAS solid $9\%\mathbf{2}-d_{13}@TPP-d_{12}$.

chemical shifts of the *p*-terphenyl carbons in solutions of **1** and **2** also display remarkable similarity. The spectrum of $15\%\mathbf{2}@TPP-d_{12}$ exhibits additional aromatic signals and two resolved *p*-carborane peaks with chemical shifts that are different from those in the spectrum of $15\%\mathbf{1}@TPP-d_{12}$. The spectrum shows a similar signal pattern as the solid-state ^{13}C spectrum of neat **2**, yet the spectra are distinctly different. The signals in the spectrum of $15\%\mathbf{2}@TPP-d_{12}$ are better resolved, and they are shifted upfield by 1–2 ppm relative to those in the ^{13}C CP MAS ssNMR spectrum of neat **2**.

In order to assign the signals in the ^{13}C spectrum of $15\%\mathbf{2}@TPP-d_{12}$, several additional solid-state experiments were performed: ^{13}C SPE MAS with a 1 s (Figure S6a of the Supporting Information) and 60 s (Figure S6b of the Supporting Information) relaxation delay, ^{13}C CP MAS NMR with a short contact time (0.2 ms) (Figure S6c of the Supporting Information), and ^{13}C CP MAS NMR spectrum with dipolar dephasing (DPD) using a 5 ms contact time (Figure S6d of the Supporting Information). The ^{13}C CP MAS NMR experiment with DPD shows only carbons that carry no protons, while the ^{13}C CP MAS with a short contact time enhances the signals of protonated carbons relative to those of

Table 1. NMR Signal Assignments for **1** (δ /ppm)

	C-1	C-2	C-3	C-4	C-5	C-6	C-7
1 in CDCl_3	140.73–140.59	139	135.49	128.97–126.70	79.2	75.96	25.83
$15\%\mathbf{1}@TPP-d_{12}$	138.88	137.26	133.7	124.58	78.15	73.03	22.62, 30.64

Table 2. Summary of Solid-State ^{13}C NMR Assignments for **2**, and the Changes in the Chemical Shift from the NMR Spectrum in CDCl_3 Solution to the 15%**2**@TPP- d_{12} CP MAS ssNMR Spectrum

solid ^a	C-1	C-2	C-3	C-4	C-5	C-6	C-7	C-8
solution ^b	l,p,q	m	c,i	a	b,d,f(?)	j,k,n,o,r,s,t	h	g
$\Delta\delta/\text{ppm}^c$	-1.7 to -2.2	-1.7	-1.4 to -1.9	-1.6	-2 to -3(?)	?	-1.4	-1.6

^aPeak assignment in ssNMR; See Figure 3. ^bPeak assignment in solution NMR; See Scheme 1. ^cDifference in chemical shifts; solid minus solution.

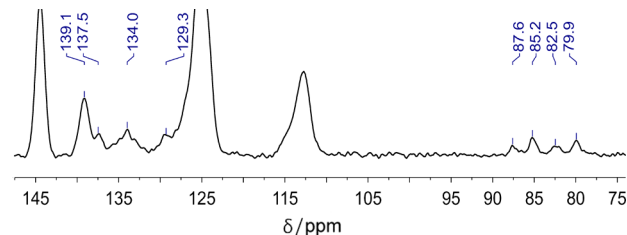
quaternary carbons. The two experiments reveal that the peaks C-1 and C-2 belong to quaternary carbons. The same peaks with identical chemical shifts are also found in the solid-state ^{13}C NMR spectrum of the inclusion compound 15%**1**@TPP- d_{12} (C-1 and C-2, Figure 3d), and they therefore belong to the four *p*-terphenyl carbons. The signal of the fifth quaternary *p*-terphenyl carbon C-3 in 15%**2**@TPP- d_{12} overlaps with that of one of the quaternary carbons of the 2,3-dichlorophenyl residue. The signals of carbons C-4 and C-5 contain contributions from the two other quaternary carbons of 2,3-dichlorophenyl, and the peak C-5 also contains at least one of the three signals of protonated carbons of 2,3-dichlorophenyl. The solid-state ^{13}C SPE MAS NMR spectrum of 15%**2**@TPP- d_{12} (Figure S6b of the Supporting Information) was recorded with a relaxation delay of $5T_1$ of the slowest relaxing carbon (12 s), and it is therefore quantitative. It shows that the peaks C-1 and C-2 contain altogether four carbons, peaks C-3 and C-4 together integrate to three, and peak C-5 also to three. The integration of the signal C-5 is not accurate due to an overlap with a TPP signal.

The solid-state ^{13}C CP MAS NMR spectrum of 9%**2**- d_{13} TPP- d_{12} (Figure 4d) only contains the signals of the 2,3-dichlorophenyl unit, as the deuteriated *p*-terphenyl carbons in TPP- d_{12} channels do not get significantly cross-polarized by any protons in the sample and are missing in the spectrum. The comparison with the 15%**2**@TPP- d_{12} ^{13}C CP MAS ssNMR spectrum confirms the assignment of the carbons C-1, C-2, and part of C-3 to *p*-terphenyl and C-4, C-5, and part of C-3 to 2,3-dichlorophenyl. The C–B peak in the spectrum of 9%**2**- d_{13} TPP- d_{12} is sharper than the C–B signal in the solid-state spectrum of 15%**2**@TPP- d_{12} ^{13}C , which has a downfield shoulder. This indicates that a significant portion of the signal from the protonated carbons of the *p*-terphenyl lies in this shoulder. The remaining aromatic signals (C-4, C-5, and part of C-3) belong to the 2,3-dichlorophenyl unit.

The comparison with the solution ^{13}C NMR spectrum of **2** suggests that the signal C-1 corresponds to the carbons C_p , $C_{p'}$, and $C_{q'}$, while the signal C-2 corresponds to C_m and a part of signal C-3 belong to C_i . Most of the protonated carbon signals are not resolved (C-6) and they overlap with the TPP peak C–B. The remaining part of peak C-3 belongs to the carbon C_a , C-4 corresponds to the carbon C_o , and a part of the peak C-5 corresponds to the carbon C_b .

All the aromatic and *p*-carborane carbons in the solid-state ^{13}C NMR spectra of 15%**2**@TPP- d_{12} display a large upfield shift with respect to solution ^{13}C NMR spectrum of **2**. The assignments and changes in the chemical shift relative to the solution spectrum are summarized in Table 2.

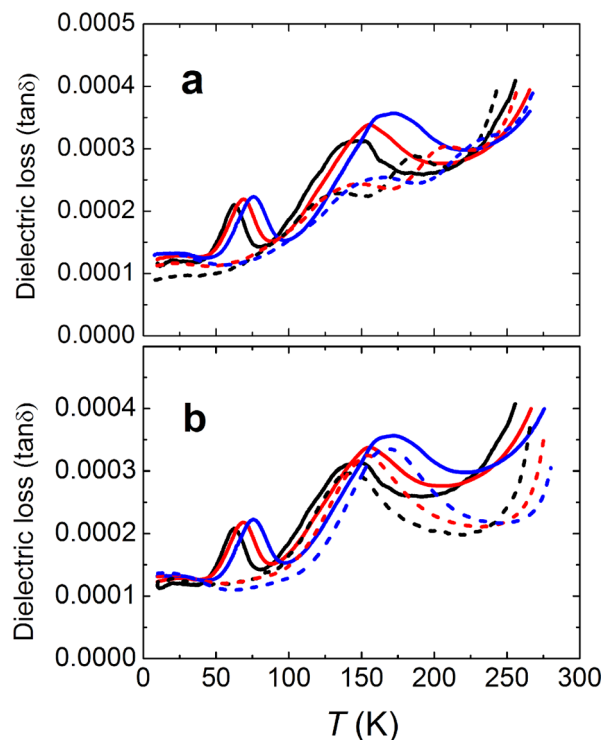
Additional information is available for an incompletely annealed sample het-15%**2**@TPP- d_{12} (Figure 5). In the solid-state ^{13}C CP MAS NMR spectrum, the four downfield quaternary *p*-terphenyl carbon signals C-1 and C-2 all show similar upfield change of the chemical shifts as in the homogeneous sample 15%**2**@TPP- d_{12} . The remaining aromatic signals are a superposition of peaks with chemical shifts similar

**Figure 5.** ^{13}C CP MAS NMR spectrum of het-15%**2**@TPP- d_{12} .

to 15%**2**@TPP- d_{12} and a similar set of signals shifted downfield relative to those found in 15%**2**@TPP- d_{12} .

The carbon atoms of the carborane unit appear doubled in this heterogeneous sample, at 79.9 and 82.5 ppm, and at 85.2 and 87.6. Heating the het-15%**2**@TPP- d_{12} sample results in an inclusion compound with the same sets of ^{13}C signals as the homogeneous 15%**2**@TPP- d_{12} sample, while the heating of a mixture of finely ground **2** and TPP- d_{12} does not yield an inclusion compound. This suggests that the inclusion compound het-15%**2**@TPP- d_{12} is not contaminated with detectable amounts of the neat rotor **2**.

Dielectric Loss Spectroscopy. In Figure 6, we show dielectric spectra taken for several samples from 8 to 300 K with applied frequencies in the audio range from 120 Hz to 12

**Figure 6.** (a) Dielectric loss spectra at 0.12 (black), 1.2 (red), and 12 (blue) kHz. Full lines: (a and b) het-15%**2**@TPP- d_{12} . Dashed lines: (a) 15%**1**@TPP- d_{12} and (b) 15%**2**@TPP- d_{12} .

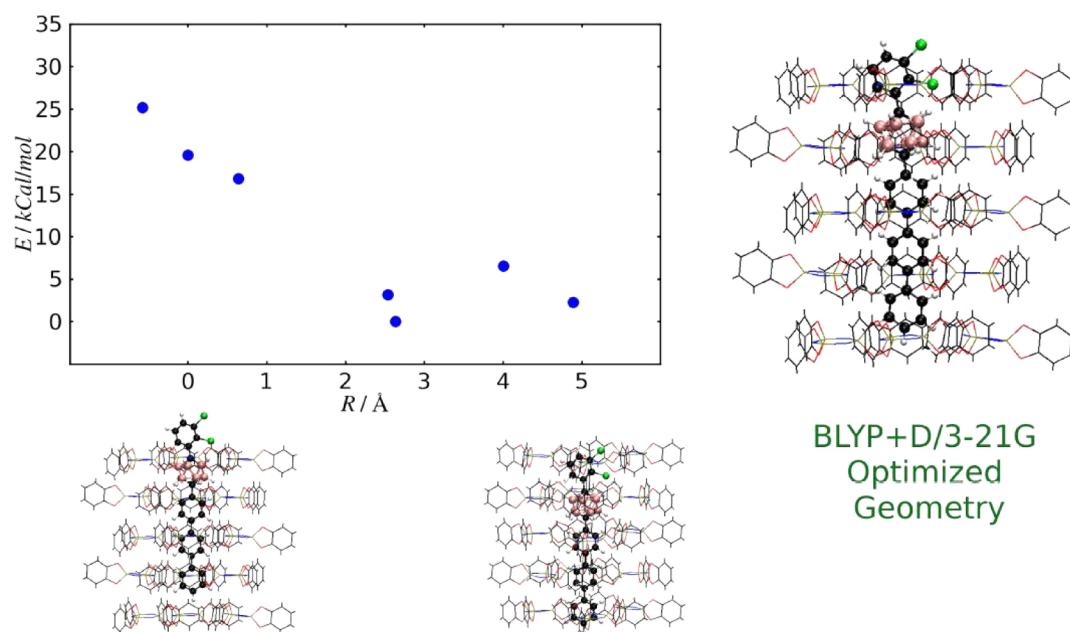


Figure 7. BLYP+D/3-21G geometry optimization of a single TPP channel with **2** inserted. The x axis is the displacement of **2** into ($R > 0$) or out of ($R < 0$), the channel along the channel axis.

kHz. The unannealed sample $\text{het-15}\%2@TPP-d_{12}$ shows two dispersing dielectric loss structures, one near 150 K, consistent with thermal activation over a barrier of 8.75 ± 0.5 kcal/mol with an attempt frequency of 1×10^{14} Hz and an asymmetry in the wells of 0.22 ± 0.02 kcal/mol, and the second near 70 K, consistent with a barrier of 3.39 ± 0.3 kcal/mol and an attempt frequency of 10^{13} Hz and a more symmetric well with only 0.09 ± 0.01 kcal/mol asymmetry. The annealed homogeneous sample $15\%2@TPP-d_{12}$ spectra show only the high temperature dielectric loss structure with a barrier of 8.52 ± 0.5 and an asymmetry of 0.26 ± 0.01 kcal/mol.

Calculations. The geometry of **2** inserted to different degrees into a channel of four layers of TPP was optimized using the BLYP+D method³¹ and the 3-21G basis set (the channel was allowed to expand or contract). The lowest minimum obtained by this method shows most of the guest molecule **2** contained inside the channel, except for a small part of the dichlorophenyl rotator (Figure 7).

DISCUSSION

In the samples examined, **1** and **2** are undoubtedly included as guests in the channels of TPP: (i) the XRD results show the exclusive presence of the hexagonal phase of TPP, with expanded lattice parameters in the plane of the layers. (ii) The CP MAS experiments exhibit cross-polarization of ^{31}P and ^{13}C atoms of fully deuterated TPP, which indicates close proximity to ^1H atoms of the guest molecules. The same signals are also observed for these atoms in SPE MAS experiments, which do not depend on cross-polarization, indicating homogeneous hexagonal structure throughout the samples, and the absence of the monoclinic form of TPP (within the sensitivity of this method). (iii) Most chemical shifts of the carbon atoms of the guest molecules observed in the inclusion compounds are displaced upfield. The following discussion depends on the firm assignments of ^{13}C NMR signals to individual carbons that were described above.

We propose that (i) the annealed $15\%2@TPP-d_{12}$ sample is homogeneous and its structure can be characterized as a near-

surface inclusion compound, with the guest molecules inside the TPP channels but abutting the surface; (ii) the unannealed $\text{het-15}\%2@TPP-d_{12}$ sample is heterogeneous and contains a fraction of the guest molecules in the near-surface position and a fraction in a surface location with the rotator extending outside the surface; and (iii) the rotator-free $15\%1@TPP-d_{12}$ sample in which the rotor only carries a methyl group is also heterogeneous, with about half of the guest molecules in an unknown position inside the TPP channels and the other half in a surface location with the methyl group extending outside the surface. In the following, we first discuss the supporting structural evidence that is provided by the complementary types of measurement, and second, we examine the compatibility of the proposals with the rotational barriers deduced from the observed dielectric spectra.

$15\%2@TPP-d_{12}$. First, we note that a 15% molar mixture in $TPP-d_{12}$ is a very close match to what one expects for a platelike crystal of TPP with rotors populating the top and bottom surfaces fully and with plate thickness just sufficient for the inserted tails to touch along the plate midplane (similar to what is shown for **1** in Figure 8d). Second, the very similar lattice parameters observed with the methyl carrying rotor $15\%1@TPP-d_{12}$ and the dipolar rotator carrying $15\%2@TPP-d_{12}$ suggests that the rotators are not important in setting lattice parameters. Such a result is expected if the rotators are in the surface layer and partly outside the crystallites. Previously reported bulk inclusion compounds of a *p*-carborane with 2,3-dichlorophenyl moieties on both of its carbons, which clearly have the 2,3-dichlorophenyl groups fully within the TPP channels,²¹ have a much expanded in-plane lattice parameter of 1.258 nm, substantially larger than $15\%1@TPP-d_{12}$ and $15\%2@TPP-d_{12}$, again consistent with the 2,3-dichlorophenyl rotator being at least partly outside the bulk channels in the latter two.

The solid-state ^{13}C CP MAS NMR spectrum of $15\%2@TPP-d_{12}$ only displays upfield changes in the chemical shifts relative to the solution ^{13}C NMR spectrum, indicating that the 2,3-dichlorophenyl rotator is located inside the $TPP-d_{12}$ channel. If the dichlorophenyl rotator were freely rotating, the T_1

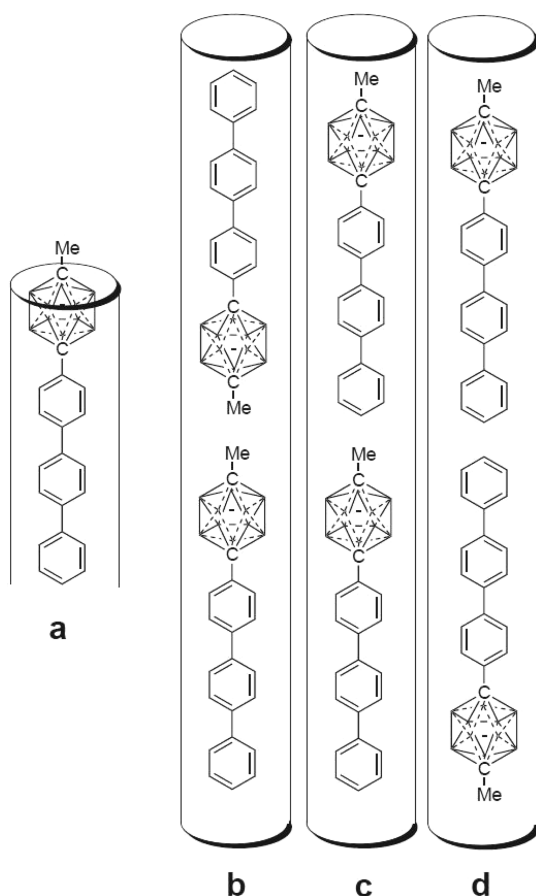


Figure 8. Possible relative orientations of **1** in a TPP- d_{12} channel.

relaxation times of these carbons should be lower than those of carbons located inside the channels. The ^{13}C SPE MAS NMR spectrum with short relaxation delay (Figure S6 of the Supporting Information) does not show any decrease in ^{13}C intensity of the shaft carbons versus the carbons of the dichlorophenyl rotator, which is also consistent with the insertion of the rotator into the channel.

A way to reconcile the apparently contradictory conclusions from XRD and the NMR methods is to postulate that 15%**2**@TPP- d_{12} is an inclusion compound in which the 2,3-dichlorophenyl rotators are inserted in the first layer, in agreement with our DFT calculations (Figure 7). The insertion of all the rotor parts, including the rotator, is likely due to a stabilizing π -stacking interactions of the 2,3-dichlorophenyl group with an expanded TPP- d_{12} channel.

Het-15%2**@TPP- d_{12} .** Figures 4 and 5 show NMR spectra for samples of neat **2**, het-15%**2**@TPP- d_{12} , and 15%**2**@TPP- d_{12} , which has received additional annealing at 70 °C to lead to a more homogeneous NMR structure. The signals associated with the carbons of the *p*-carborane cage appear as two peaks in the spectrum of 15%**2**@TPP- d_{12} and are both shifted upfield relative to the solution spectrum of **2**. In het-15%**2**@TPP- d_{12} , however, these two peaks are split into pairs of shifted and unshifted peaks, indicating the presence of two populations of rotor molecules. One of them is the same as in 15%**2**@TPP- d_{12} , with the carborane fully inserted into TPP, and the other has the carborane and therefore also the rotator outside. Annealing to 70 °C produces a homogeneous population where all carboranes are inserted at least as far as the first TPP layer.

15%1**@TPP- d_{12} .** The near identity of the XRD results for this inclusion compound and for 15%**2**@TPP- d_{12} suggests that **1** inserts its *p*-terphenyl shaft and the attached carborane cage inside the TPP channel, and this agrees perfectly with the upfield shift of all its carbon atoms in the NMR spectrum. The only exception is the methyl carbon signal, which is split into two peaks, showing that the methyl group is in two distinct environments. One of the peaks is shifted upfield, by 3.2 ppm with respect to the solution spectrum of **1** and has the methyl group inside the TPP channel. We cannot tell if it is a true bulk inclusion or if these molecules of **1** reside near the surface. The other peak is shifted strongly downfield by 4.8 ppm, and we attribute this to a surface inclusion with the methyl groups just above the surface, in the deshielding zone of the channel (Figure 8a). It could be argued that the molecules of **1** can possibly fill the channel with three different relative orientations as shown in Figure 8 and that the remarkable 4.8 ppm downfield change in the chemical shift of the methyl carbon is due to deshielding by the terminal *p*-terphenyl phenyl group of a neighboring guest inside the channel (Figure 8c), but we consider it highly unlikely. Many solid-state ^{13}C NMR spectra of bulk inclusion compounds are known^{30,32,33} and no such strong effect on the chemical shift has ever been observed. It is remarkable that application of dipolar dephasing (Figure 3c) suppressed both methyl signals despite the fast rotation that would be expected for such a group. In order to remove first order dipolar coupling, any motion must be isotropic, as well as faster than the magnitude of the decoupling energy. In addition, since this methyl group is rather isolated, the C–H dipolar coupling could be behaving as an isolated dipolar spin system, in which the coherence nutates as a function of dephasing delay. It is possible that the delay chosen in this experiment was at the zero-crossing of this nutation of the CH dipolar coupling.

In spite of the much smaller size of its rotator, **1** thus appears to be more inclined to form a true surface inclusion with the rotator outside than **2** does. We suggest that this is due to a favorable π – π stacking interaction of the 2,3-dichlorophenyl rotator of **2** with the channel walls, which is absent in case of the methyl in **1**.

Dielectric Spectroscopy. To help isolate the behavior of the dipolar rotors from the general dielectric response, we compare the dielectric loss spectra of 15%**2**@TPP- d_{12} and het-15%**2**@TPP- d_{12} with those of the nonpolar 15%**1**@TPP- d_{12} (Figure 4). This material shows low levels of dielectric loss and serves as a good indication of overall contributions of TPP and the carborane plus terphenyl moieties in the guest. Both 15%**2**@TPP- d_{12} and het-15%**2**@TPP- d_{12} show substantial new dielectric loss peaks, attributed to the presence of 2,3-dichlorophenyl dipolar rotators. While the former has only a barrier peak at 8.52 ± 0.5 kcal/mol, the latter has dipoles in two distinct environments, with barriers to rotation of 8.75 ± 0.5 kcal/mol and 3.39 ± 0.3 kcal/mol.

The considerable ~ 8.6 kcal/mol barrier observed in both samples suggests that the 2,3-dichlorophenyl rotator faces significant steric hindrance to rotation. Given its size, this would be expected if it is included in the first layer of TPP. The value is consistent with the rotational barriers found for the 2,3-dichlorophenyl rotator in a bulk TPP inclusion compound of di(1,12-dichlorophenyl)-*p*-carborane,²¹ which carries the 2,3-dichlorophenyl rotator on both antipodal carbons. Their heights are ~ 5.4 , ~ 6.7 , and ~ 9.3 kcal/mol (attributed to three different local environments). Here, the TPP in-plane lattice parameter is expanded to 1.254 nm to fully

accommodate the carborane and the rotator. The dielectric measurement thus provides further evidence for a near-surface inclusion of the rotor **2**.

The het-15%2@TPP- d_{12} sample has an additional population of dipoles with a much lower barrier of ~ 3.4 kcal/mol. These must be the rotators observed by NMR to be located further outside the TPP surface. The height of this barrier is still clearly in excess of the intrinsic intramolecular rotational barrier, most likely because one of the chlorine substituents on the rotator remains too close to the TPP surface.

Mechanism of Formation of the Inclusion Compounds. The expanded lattice parameters in these and other inclusion compounds formed by ball milling suggest a simple explanation of how self-assembly may occur: any surface perpendicular to the c axis direction of an empty TPP crystallite that becomes populated with rotors, a necessary step for formation of either a surface or bulk inclusion compound, will be subjected to a substantial strain. The strain may naturally cause the crystallite to fracture along a plane perpendicular to the c axis into a populated and an unpopulated part. This process will take place on both sides of a crystallite plate, and sequential fracturing and population during ball milling may then lead to the observed structure.

CONCLUSIONS

The molecular rotors **1** and **2** form inclusion compounds with TPP. Heterogeneous samples with two dominant environments for the guest species were obtained from both, and a homogeneous sample with a single dominant guest environment was obtained from **2**. In the homogeneous sample, 15%2@TPP- d_{12} , the entire rotor molecule is inserted but remains at the surface with the rotator in the first TPP layer, forming what we term a near-surface inclusion compound. This same structure was derived independently from DFT modeling. As a result of rotator embedding, its rotation is considerably hindered (~ 8.6 kcal/mol).

The heterogeneous sample obtained from **2** contains this same structure as one dominant component. The other main component has the rotator protruding outside the TPP surface but apparently not far enough to avoid all friction against the surface, and it turns with a barrier of ~ 3.4 kcal/mol.

The inclusion compound 15%1@TPP- d_{12} shows an interesting behavior: it has about equal populations of a structure with the methyl inserted and a structure with the methyl outside. Clearly, although **1** has the same shaft and the stopper as **2**, its methyl group does not show as much affinity for the channel as the 2,3-dichlorophenyl group of **2** does. This is attributed to a weaker stabilizing interaction between the TPP channel and the methyl group, which is too small for a van der Waals contact with the channel walls, as opposed to the 2,3-dichlorophenyl group, which nominally is too large. This observation provides an important lesson about the design of the rotator group in designing rotors for surface inclusion compounds.

In summary, we have prepared TPP inclusion samples with interesting structures and have learned more about the way the inclusion works, but we have not produced a homogeneous sample with a sufficiently small barrier to rotation to show collective dielectric behavior. Apparently, the stoppers need to be even larger than p -carborane, or we need to work with larger crystal facets that might make it harder for the guest molecules to expand the lattice and force their way inside the TPP channels. It might also be helpful to choose rotators that have less affinity for the inside of the TPP channel.

EXPERIMENTAL PART

X-ray Diffraction. The X-ray powder patterns were taken with a system based on a Rigaku Ultrax18 rotating anode generator. It uses a curved silicon multilayer monochromator to produce Cu $K\alpha$ radiation at wavelength $\lambda = 0.15418$ nm. Powder samples, loaded into 1.0 mm diameter borosilicate glass capillaries with a wall thickness of 10 μm , were mounted on a Huber four-circle goniometer. The scattered X-rays were measured with a sodium iodide scintillator point detector that was moved in a horizontal plane, by an angle 2θ with respect to the direction of the incident X-rays, to scan the Bragg scattering profile. The resolution of the instrument, in its usual configuration, is $q_{\text{res}} \approx 0.003 \text{ \AA}^{-1}$.

DSC. The DSC measurements were performed with a TA Instruments DSC Q200 apparatus.

NMR. Solution spectra were obtained with Varian INOVA-400 and INOVA-500 and Bruker Avance-III 300 NMR spectrometers. Solid-state NMR measurements were performed with a Varian INOVA-400 (400 MHz) NMR spectrometer equipped with 5 and 4 mm solid-state NMR probes. Magic-angle sample spinning (MAS) used spinning frequencies of 12.5–14 kHz for CPMAS and SPE-MAS experiments. For dipolar dephasing experiments, spinning speeds of 5–6 kHz were used to allow adequate time for dipolar dephasing and chemical shift refocusing within one rotor period. Cross-polarization experiments were performed using spin-lock fields of 72–75 kHz, and ramped-amplitude cross-polarization (RAMP-CP) transfer of magnetization was applied. For both cross-polarization and single-pulse excitation (SPE) experiments, broadband TPPM-modulated ^1H decoupling was used.

Chemical shifts for solid-state ^{13}C and ^{31}P nuclei were calibrated using the absolute referencing method, relative to the absolute frequency of 0.0 ppm in ^1H NMR.³⁴ As a check for this referencing method, external samples of hexamethylbenzene (HMB, ^{13}C) and triphenylphosphine (^{31}P) were acquired and calibrated using this referencing method, yielding ^{13}C chemical shifts of HMB of 132.2 and 17.4 ppm. The observed chemical shift of pure, solid triphenylphosphine using the absolute referencing method was -8.5 ppm.

Dielectric Spectroscopy. The powder samples were loaded onto the surface of coplanar interdigitated electrode capacitors fabricated by gold metallization on fused silica substrates (each with 50 fingers separated by $\sim 10 \mu\text{m}$ gaps). Nominal capacitor values for the empty capacitors were near 1 pF and dielectric loss tangents were at or below the 10^{-5} level.³⁵ An Andeen–Hagerling capacitance bridge was used to measure the dielectric loss and capacitance with a sinusoidal alternating voltage (1.8–5 V and 0.12–12 kHz) applied on the capacitor. Data were taken continuously with the temperature slowly changing between 7 K and room temperature. The curves were averaged over heating and cooling steps and smoothed.

Calculations. The geometry of a single channel composed of four layers of TPP with a guest molecule **2** (Figure 7) was optimized using BLYP with dispersion and the 3-21G basis set using Terachem 1.5.³¹ The channel was only partially constrained during the optimization to allow for expansion or contraction. The initial geometries were generated from the $R = 0$ geometry shown in Figure 7 by moving the guest by multiples of 0.1 nm either inside or outside the channel along its axis, and they were further optimized into the nearest local minimum.

Synthesis. General Methods. Air-sensitive reactions were carried out under argon, using standard Schlenk techniques. Tetrahydrofuran was distilled from Na/K under argon. Pyridine was distilled from calcium hydride under argon. Triethylamine was distilled from calcium hydride or from sodium/benzophenone under argon. Dimethylformamide was distilled from calcium hydride under reduced pressure. Cuprous chloride was purchased from Sigma-Aldrich in sealed ampules and handled in a glovebox. Only pure white cuprous chloride was used in reactions. All chemicals except for the p -carborane (Katchem) were purchased from Sigma-Aldrich and used as received.

Standard procedures were used to characterize all new compounds. IR spectra were recorded with a Nicolet Avatar 360 FT-IR spectrophotometer using KBr that had been dried at 200 $^\circ\text{C}$ for 24

h. UV-vis spectra were recorded with a Hewlett-Packard 8452A spectrometer. A Hewlett-Packard 5989B mass spectrometer was used to record mass spectra. Elemental analyses were performed by Columbia Analytical Services, Tucson, AZ.

Inclusion Compound Preparation. The inclusion compounds were prepared by ball milling of empty hexagonal TPP- d_{12} with the neat rotor followed by annealing at 70 to 75 °C and repetition of the two steps (15%1@TPP- d_{12} : ball milling for 80 min, annealing for 1 day, ball milling for 30 min, and annealing for 3 days; 15%2@TPP- d_{12} : ball milling for 120 min, annealing for 1 day, ball milling for 30 min, and annealing for 3 days).

1-Methyl-12-(2,3-dichlorophenyl)-*p*-dicarba-closo-dodecaborane (1). A dry Schlenk flask (25 mL) was equipped with a septum and a magnetic stir bar. It was charged with 3^{22} (200.0 mg, 0.537 mmol, 1.0 equiv), evacuated, and filled with argon (3 \times). Anhydrous THF (20 mL) was added through the septum, and the mixture was cooled in an acetone/dry ice bath. After 5 min, 1.6 M solution of *n*-BuLi in hexanes (0.40 mL, 0.644 mmol, 1.2 equiv) was added to the solution, which was then allowed to warm to room temperature. After 30 min of stirring at room temperature, the mixture was again placed in an acetone/dry ice bath, and methyl iodide (152.3 mg, 1.074 mmol, 2.0 equiv) was added. The resulting mixture was allowed to warm to room temperature, and it was stirred overnight (16 h). It was quenched with a few drops of water, and the solvents were removed under reduced pressure. The solid residues were dissolved in dichloromethane (100 mL), washed with 5% hydrochloric acid (20 mL) and water (2 \times 20 mL), and the organic layer was dried over anhydrous sodium sulfate, filtered, and the solvents were removed under reduced pressure. Crystallization from cyclohexane provided 163.7 mg (79%) of white crystals, mp (CH₂Cl₂) 261 °C. ¹H NMR (300 MHz, CDCl₃): δ 7.68–7.55 (m, 6H), 7.48–7.41 (m, 4H), 7.39–7.32 (m, 1H), 7.28 (dt, *J* = 7.1, 1.3 Hz, 2H), 1.42–3.5 (m, 10H), 1.48 (s, 3H). ¹³C{¹H} NMR (75 MHz, CDCl₃): δ 140.73 (s), 140.68 (s), 140.59 (s), 139.00 (s), 135.49 (s), 128.96 (s), 127.83 (s), 127.66 (s), 127.56 (s), 127.49 (s), 127.17 (s), 126.70 (s), 79.22 (s), 75.99 (s), and 25.83 (s). ¹¹B{¹H} NMR (96 MHz, CDCl₃): δ –11.97 (s). IR (KBr, cm^{–1}): 429, 445, 510, 528, 566, 579, 600, 620, 666, 700, 719, 730, 767, 813, 837, 864, 882, 979, 1004, 1032, 1069, 1115, 1133, 1169, 1196, 1253, 1309, 1318, 1331, 1361, 1387, 1396, 1412, 1445, 1482, 1496, 1503, 1526, 1542, 1558, 1568, 1580, 1595, 1953, 2600, 2609, 2873, 2939, 2987, 3027, 3047, 3075, 3085. HRMS (ESI[–]): 422.2718 (calcd for MCl[–]: 422.2718). UV-vis (CH₂Cl₂, nm) λ_{\max} (ϵ_{\max}): 286 (43980). Elemental analysis: calcd C, 65.25%; H, 6.78%. Found: C, 64.86%; H, 7.18%.

1-(4-*p*-Terphenyl)-12-(2,3-dichlorophenyl)-*p*-dicarba-closo-dodecaborane (2). A pressure Schlenk flask (25 mL), equipped with a pressure valve, a magnetic stir bar, a septum, and a hose connector, was charged with **3** (300 mg, 0.804 mmol, 1.0 equiv) and with cuprous chloride (103.4 mg, 1.045 mmol, 1.3 equiv) under argon. THF (10 mL) was added through the septum under argon, and the resulting mixture was cooled in an acetone/dry ice bath. After 5 min of stirring, *n*-BuLi (1.6 M solution in hexanes, 0.603 mL, 0.965 mmol, 1.2 equiv) was added dropwise under argon. The reaction mixture was stirred for 15 min at –78 °C and then for 30 min at room temperature. Anhydrous pyridine (1 mL) was added to the mixture, and it was stirred until all the cuprous chloride dissolved. The solvents were removed under reduced pressure and the flask was filled with argon. After that, a suspension/solution of the 1,2-dichloro-3-iodobenzene (329 mg, 1.206 mmol, 1.5 equiv) in anhydrous DMF (8 mL) was added under argon. The resulting mixture was heated in a closed vessel at 120 °C for 24 h and then at 140 to 150 °C for 24 to 48 h. After the reaction was complete, the solvents were removed under reduced pressure and the solids were dissolved in dichloromethane (100 mL), washed with 5% hydrochloric acid (50 mL), with 10% ammonium hydroxide (2 \times 50 mL), and with water (50 mL). The organic layer was dried over anhydrous sodium sulfate, filtered, and concentrated under reduced pressure. The product was purified by chromatography in pentanes and toluene (3/1 to 2/1) on silica gel to yield 399 mg (96%) of pure product (white crystals), mp (CH₂Cl₂): 234 °C. ¹H NMR (500 MHz, CDCl₃): δ 7.69–7.57 (m, 7H), 7.50–7.44 (m, 4H), 7.41 (dd, *J* = 7.9, 1.5 Hz, 1H), 7.38 (d, *J* = 7.4 Hz, 1H), 7.35–7.31 (m,

2H), 7.08 (dt, *J* = 8.1 Hz, 1H), 3.63–1.99 (m, 10H). ¹³C{¹H} NMR (75 MHz, CDCl₃): δ 141.08 (s), 140.69 (s), 140.67 (s), 138.91 (s), 135.93 (s), 135.39 (s), 134.20 (s), 131.48 (s), 131.05 (s), 130.71 (s), 128.98 (s), 127.70 (s), 127.63 (s), 127.60 (s), 127.51 (s), 127.18 (s), 126.82 (s), 126.67 (s), 86.52 (s), 81.80 (s). ¹¹B{¹H} NMR (96 MHz, CDCl₃): δ –12.28 (s). IR (KBr, cm^{–1}): 490, 528, 534, 565, 606, 616, 660, 697, 713, 739, 754, 763, 787, 919, 843, 865, 870, 905, 914, 931, 966, 981, 1002, 1015, 1037, 1047, 1061, 1082, 1122, 1132, 1164, 1194, 1204, 1255, 1267, 1314, 1330, 1358, 1397, 1450, 1485, 1504, 1558, 1581, 1594, 1729, 1920, 1950, 1965, 2606, 2663, 2852, 2922, 2955, 3029, 3048, 3055, 3110. HRMS (ESI[–]): 552.2105 (calcd for MCl[–]: 552.2083). UV-vis (CH₂Cl₂, nm) λ_{\max} (ϵ_{\max}): 290 (46840). Elemental analysis: calcd C, 60.34%; H, 5.06%. Found: C, 60.13%; H, 5.17%.

Synthesis of 4-iodo-*p*-terphenyl-*d*₁₃ (4). A 5 mL glass vial was charged with *p*-terphenyl-*d*₁₄ (250.0 mg, 1.023 mmol, 1.0 equiv), silver nitrate (700.0 mg, 4.250 mmol, 4.15 equiv), iodine (1.05 g, 4.132 mmol, 4.0 equiv), anhydrous acetonitrile (0.2 mL), and a stir bar. The vial was closed with a lid with a Teflon liner, and the resulting paste was shaken vigorously for 12 h. It was then allowed to sit at room temperature for 48 h. The mixture was transferred into a separatory funnel with dichloromethane (100 mL), washed with 10% ammonium hydroxide (2 \times 80 mL), 5% sodium thiosulfate (2 \times 50 mL), and water (80 mL). The organic layer was dried over anhydrous sodium sulfate, filtered, and the solvents were removed under reduced pressure. The crude product was purified by two Kugelrohr sublimations at 80 to 120 °C (50 to 80 mTorr) to yield 245.9 mg (65%) of pure white crystalline product. ¹H NMR (300 MHz, CDCl₃): δ 7.81 (s), 7.70 (s), 7.66 (s), 7.48 (s), 7.41 (s), 7.39 (s).

Synthesis of 3-*d*₁₃. The product was prepared by the same procedure as the nondeuteriated version **3**,²² starting with **4**. Kugelrohr sublimation (140 °C/30 mTorr) was used in place of the crystallization. The yield of the product was 89%. ¹H NMR (300 MHz, CDCl₃): δ 7.65 (s), 7.63 (s), 7.60 (s), 7.46 (s), 7.45 (s), 7.36 (s), 7.30 (s), 3.68–0.75 (m).

Synthesis of 2-*d*₁₃. The same procedure as for synthesis of **2** was employed, starting with **3-*d*₁₃**. The yield was 94%. ¹H NMR (300 MHz, CDCl₃): δ 7.59 (dd, *J* = 8.4, 1.4 Hz, 1H), 7.41 (dd, *J* = 7.9, 1.4 Hz, 1H), 7.07 (t, *J* = 8.1 Hz, 1H), 2.93 (s, 5H), 2.70 (s, 5H).

■ ASSOCIATED CONTENT

📄 Supporting Information

DSC traces, NMR assignments, relaxation times. This material is available free of charge via the Internet at <http://pubs.acs.org>.

■ AUTHOR INFORMATION

✉ Corresponding Author

*E-mail: michl@eefus.colorado.edu.

📄 Notes

The authors declare no competing financial interest.

■ ACKNOWLEDGMENTS

This work was supported in Prague by the European Research Council under the European Community's Seventh Framework Programme (FP7/2007-2013) ERC Grant 227756 and by the Institute of Organic Chemistry and Biochemistry, Academy of Sciences of the Czech Republic RVO: 61388963, and in Boulder by the National Science Foundation under Grant CHE 0848663.

■ REFERENCES

- (1) Kottas, G. S.; Clarke, L. I.; Horinek, D.; Michl, J. *Chem. Rev.* **2005**, *105*, 1281.
- (2) Khuong, T.-A. V.; Nunez, J. E.; Godinez, C. E.; Garcia-Garibay, M. A. *Acc. Chem. Res.* **2006**, *39*, 413.
- (3) Horansky, R. D.; Magnera, T. F.; Price, J. C.; Michl, J. In *Controlled Nanoscale Motion, Lecture Notes in Physics*; Linke, H.; Månsson, A., Eds.; Springer: Berlin, 2007; Vol. 711, p 303.

- (4) Crowley, J. D.; Kay, E. R.; Leigh, D. A. *Intelligent Materials*; Shahinpoor, M., Schneider, H.-J., Eds.; 2008; Vol 1, p 1–47.
- (5) Garcia-Garibay, M. A. *Nat. Mater.* **2008**, *7*, 431.
- (6) Michl, J.; Sykes, E. C. H. *ACS Nano* **2009**, *3*, 1042.
- (7) Augulis, R.; Klok, M.; Feringa, B. L. *Phys. Status Solidi C* **2009**, *6*, 181.
- (8) Winston, E. B.; Lowell, P. J.; Vacek, J.; Chocholousova, J.; Michl, J.; Price, J. C. *Phys. Chem. Chem. Phys.* **2008**, *10*, 5188.
- (9) Horansky, R. D.; Clarke, L. I.; Price, J. C.; Khuong, T.-A. V.; Jarowski, P. D.; Garcia-Garibay, M. A. *Phys. Rev. B* **2005**, *72*, 014302.
- (10) Rodriguez-Molina, B.; Ochoa, M. E.; Farfan, N.; Santillan, R.; Garcia-Garibay, M. A. *J. Org. Chem.* **2009**, *74*, 8554.
- (11) Gimzewski, J. K.; Joachim, C.; Schlittler, R. R.; Langlais, V.; Tang, H.; Johannsen, I. *Science* **1998**, *281*, 531.
- (12) Zheng, X.; Mulcahy, M. E.; Horinek, D.; Galeotti, F.; Magnera, T. F.; Michl, J. *J. Am. Chem. Soc.* **2004**, *126*, 4540.
- (13) Tierney, H. L.; Murphy, C. J.; Jewell, A. D.; Baber, A. E.; Iski, E. V.; Khodaverdian, H. Y.; McGuire, A. F.; Klebanov, N.; Sykes, E. C. H. *Nat. Nanotechnol.* **2011**, *6*, 625.
- (14) Delden, R. A.; ter Wiel, M. K. J.; Pollard, M. M.; Vicario, J.; Koumura, N.; Feringa, B. L. *Nature* **2005**, *437*, 1337.
- (15) Clarke, L. I.; Horinek, D.; Kottas, G. S.; Varaksa, N.; Magnera, T. F.; Hinderer, T. P.; Horansky, R. D.; Michl, J.; Price, J. C. *Nanotechnology* **2002**, *13*, 533.
- (16) Carroll, G. T.; Pollard, M. M.; van Delden, R.; Feringa, B. L. *Chem. Science* **2010**, *1*, 97.
- (17) Rodriguez-Molina, B.; Farfan, N.; Romero, M.; Mendez-Stivalet, J. M.; Santillan, R.; Garcia-Garibay, M. A. *J. Am. Chem. Soc.* **2011**, *133*, 7280.
- (18) Mulcahy, M. E.; Magnera, T. F.; Michl, J. *J. Phys. Chem. C* **2009**, *113*, 20698.
- (19) Rozenbaum, V. M.; Ogenko, V. M.; Chuiko, A. A. *Phys.-Usp.* **1991**, *34*, 883.
- (20) Kobr, L.; Zhao, K.; Shen, Y.; Comotti, A.; Bracco, S.; Shoemaker, R. K.; Sozzani, P.; Clark, N. A.; Price, J. C.; Rogers, C. T.; Michl, J. *J. Am. Chem. Soc.* **2012**, *134*, 10122.
- (21) Kobr, L.; Zhao, K.; Shen, Y.; Polívková, K.; Shoemaker, R. K.; Clark, N. A.; Price, J. C.; Rogers, C. T.; Michl, J. *J. Org. Chem.* **2013**, *78*, 1768.
- (22) Kobr, L.; Zhao, K.; Shen, Y.; Shoemaker, R. K.; Rogers, C. T.; Michl, J. *Adv. Mater.* **2013**, *25*, 443.
- (23) Allcock, H. R.; Siegel, L. A. *J. Am. Chem. Soc.* **1964**, *86*, 5140.
- (24) Hurdís, E. C.; Smyth, C. P. *J. Am. Chem. Soc.* **1942**, *64*, 2212.
- (25) Debye, P. *Polar Molecules*; Dover Publications, Inc.: New York, 1929.
- (26) Fröhlich, H. *Theory of Dielectrics: Dielectric Constant and Dielectric Loss*, 2nd ed.; Clarendon Press: Oxford, 1958.
- (27) Daniel, V. V. *Dielectric Relaxation*; Academic Press: New York, 1967.
- (28) Comotti, A.; Simonutti, R.; Catel, G.; Sozzani, P. *Chem. Mater.* **1999**, *11*, 1476.
- (29) Allcock, H. R.; Levin, M. L.; Whittle, R. R. *Inorg. Chem.* **1986**, *25*, 41.
- (30) Comotti, A.; Simonutti, R.; Stramare, S.; Sozzani, P. *Nanotechnology* **1999**, *10*, 70.
- (31) Umfítsev, I. S.; Martínez, T. J. *J. Chem. Theory Comput.* **2009**, *5*, 2619.
- (32) Brustolon, M.; Barbon, A.; Bortolus, M.; Maniero, A. L.; Sozzani, P.; Comotti, A.; Simonutti, R. *J. Am. Chem. Soc.* **2004**, *126*, 15512.
- (33) Sozzani, P.; Comotti, A.; Bracco, S.; Simonutti, R. *Angew. Chem., Int. Ed.* **2004**, *43*, 2792.
- (34) Harris, R. K.; Becker, E. D.; Cabral de Menzes, S. M.; Grainger, P.; Hoffman, R. E.; Zilm, K. W. *Pure Appl. Chem.* **2008**, *80*, 59.
- (35) Underwood, J. M.; Price, J. C. *Rev. Sci. Instrum.* **2008**, *79*, 093905.